Thermal model for a microhot plate used in a MEM gas sensor

M. Alfredo Reyes-Barranca[a], J.L. González-Vidal[b], and A. Tavira-Fuentes[a]
[a]*Department of Electrical Engineering, CINVESTAV-IPN, MEXICO, D.F., Mexico.*
[b]*C.I.T.I.S., Universidad Autónoma del Estado de Hidalgo,*
Carretera Pachuca-Tulancingo Km. 4.5, Pachuca Hidalgo, Mexico 42076.
e-mail: mreyes@cinvestav.mx

Recibido el 3 de mayo de 2007; aceptado el 28 de junio de 2007

A thermal analytical model for a MEM gas sensor is presented and compared with an electrical circuit equivalent model. The objective is to study the temperature performance of the microhot plate configured within a MEM structure used for gas sensing. From this, it is possible to determine the magnitude of the electrical current that must be applied to the polysilicon heater on regard of its dimensions and materials used, for instance, when the sensor structure is fabricated with a MEMS technology compatible with CMOS integrated circuits fabrication. Results are presented where the response time and temperature level, as a function of applied current, can be determined. The model presented can be used as a base for designing microhot plates operating in gas sensors, where temperatures in the order of 300°C are needed and that will be integrated monolithically with associated electronics, with constraints as minimum power dissipation.

Keywords: MEMS; microhot plate; thermal conductivity; electro-thermal response.

En este trabajo se presenta un modelo analítico térmico para un microsensor de gas MEM y, además se compara con un modelo de circuito eléctrico equivalente, con el objetivo de estudiar el comportamiento térmico de una micro placa caliente de una estructura MEM utilizada en el sensado de gases. Por lo anterior, es posible determinar la magnitud de la corriente eléctrica que debe ser aplicada a un micro calefactor de polisilicio, considerando sus dimensiones y los materiales utilizados; por ejemplo, cuando la estructura del sensor es fabricada con tecnología MEMS, la cual es compatible con la fabricación de circuitos integrados CMOS. Los resultados mostrados son el tiempo de respuesta y nivel de temperatura como función de la temperatura corriente aplicada. El modelo presentado puede ser aplicado como base para el diseño de micro placas calientes usadas en sensores de gases, donde se necesitan temperaturas en el orden de los 300°C, dichos sensores de gas serán integrados monolíticamente con su electrónica asociada correspondiente, considerando un consumo de potencia mínima.

Descriptores: MEMS; microplaca caliente; conductividad térmica; respuesta electrotérmica.

PACS: 82.47.Rs; 82.45.Mp; 85.40-e

1. Introduction

Gas sensing is a main activity when monitoring toxicity levels or pollution environments, for instance. A variety of gas sensors are offered commercially that depend on the type of gas, either oxidizing or reducing gas. Also, the operating principle can be based on Taguchi configurations or thin metal oxides layers, like SnO_2 or ZnO. Actually, work is still in course to study different materials that can be feasible to fabricate gas sensors in a vast variety of applications as toxic o explosive gas detection [1], or for electronic noses sensing even organic compounds [2]. Most of the efforts are directed to conceive compact units that integrate the sensor and the processing signal electronics in the same chip, reducing important issues as costs and power dissipation, and also that can be readily processed in batch [3-10].

One kind of gas sensor is actually the *high temperature chemioresistor sensor* [11], whose structure is formed by a heater beneath a microhot plate (MHP) and a thin metal oxide layer, with operating temperatures of 200-600°C. This heating is necessary for the reaction between the film and the gas, to take place. The MHP can be considered as the heart of the sensor, since it delivers the temperature necessary to activate the sensing mechanism and stores the charge within the metal oxide layer, as a function of temperature and gas concentration. As the trend is to integrate monolithically the sensor and the electronics, this range of temperatures is not affordable for an electronic circuit, so some kind of isolation must be conceived to allow the operation of both items in a same substrate. What can make this possible is the micro-electro-mechanical-systems (MEMS) technology, taking advantage of the volumetric micromachining and creating a suspended diaphragm where the sensor structure is made on. Figure 1 shows a cross section of such a structure, with Si as the substrate and different layers of polysilicon, silicon dioxide and metal oxide. An anisotropic etching of the substrate is performed from the surface to the volume, leaving a cavity below the suspended structure and in practice, thermally isolating all the surroundings in a high degree. This way, any kind of signal processing electronics can be integrated near the sensor with no problem and achieving the purpose of a monolithic integration of the sensor system. Another concern to be considered when designing this kind of systems is to lower the power dissipation, even more if one of the purposes is to implement a portable measuring device. Here, parameters such as the structure dimensions and materials used, define the performance in this direction. So, it is important to consider the role played by them, the same way as how the structure is laid-out, to predict the thermal operation of the microhotplate with certain initial and boundary conditions imposed by the design, then having the possibility

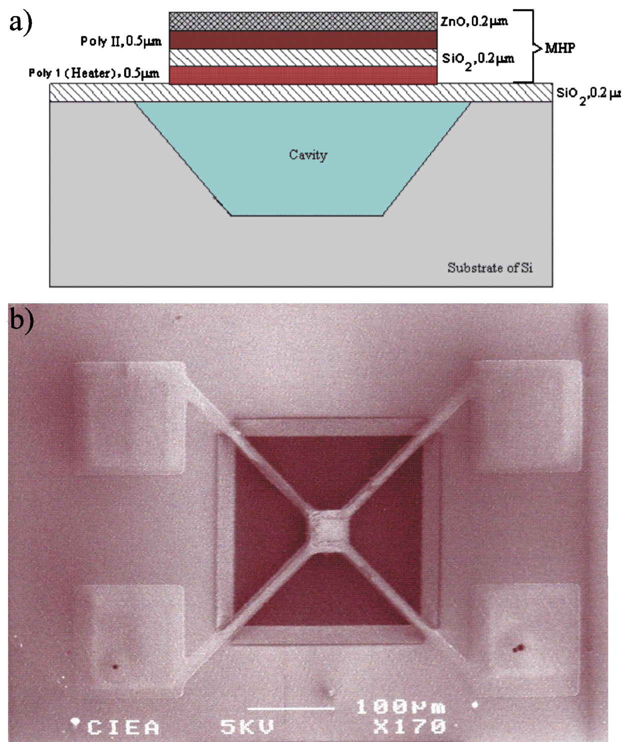

FIGURE 1. Microhot plate structure used in a MEM gas sensor, a) cross section; b) SEM micrograph.

to optimize it. In this paper, a model to study the thermal performance of a particular structure is presented, but can be adapted to any desired geometry or material of the microhot plate.

Figure 1 shows the characteristics of a particular technology that offers two polysilicon layers (PolyI and PolyII), that are separated by a layer of silicon dioxide (SiO_2). The outermost layer is the metal oxide sensor layer. PolyI is used as the heater and PolyII is a layer whose function is to collect the charge due to the chemical reaction over the sensing layer, creating a potential that can be transferred to a MOSFET gate, for instance.

2. Electro-thermal model of the MEM gas sensor

As mentioned before, heating is an important issue in the performance of the gas sensor. This can be easily achieved by Joule heat generation in a resistive element as polysilicon, the material from which the heater can be done and being compatible with CMOS integrated circuits technology. Conducting a controlled electric current through the polysilicon heater, temperature can be controlled as well [12]. Also, having a good thermal isolation to the surroundings, high temperatures can be achieved with low power consumption [13]. However, since the materials and the fabrications steps used in the MHP, are predefined by the standard technology, this could drive to some limitations in terms of the performance and reliability of the sensor. As a consequence, it is important to study the thermal performance of the MHP in those terms. Then, it is useful to have a model that describes the thermal behavior of the device in order to characterize parameters as thermal efficiency, thermal time constant and power dissipation, hence having the chance to optimize the design of the structure, as well as the design of the control and read-out circuits.

Therefore, the heat transference model in devices can be the base in the development of the desired model for the MHP. The former is based in the solution of the equation for heat conduction [4] and approximations from equivalent circuit models. These are widely used as thermal models due to their easy implementation in circuit simulators as SPICE and from where semiconductor devices are traditionally analyzed. A mapping between electric and thermal behavior is simple, although solutions are for one dimension geometries.

2.1. Electro-thermal equivalent circuit

Heat conduction processes can be modeled using two important parameters relating material properties, as thermal resistance and thermal capacitance, giving the opportunity to derive electric models using these elements, from where temperature variations over different points in the system, can be calculated. Therefore, an electric analogy can be used to study thermal performance of such systems as the one considered in this study. Here it is important to remember the

TABLE I. Thermal to electric parameter equivalence.

Thermal parameter	Electrical parameter
Temperature: T (°C)	Voltage: V(V)
Heat flow, Power P (W)	Current: I(A)
Heat: Q (J = W-sec)	Charge: Q (C = A-sec)
Resistance: R (°C/W)	Resistance: R (Ω = V/A)
Conductance: G (W/°C)	Conductance: G (S = Ω^{-1})
Capacitance: C (J/K)	Capacitance: C (F = A-sec/V)
Thermal resistivity: ρ_{th}(°C-m/W)	Electric resistivity: ρ_{e1} (Ω-m)
Thermal conductivity: κ (W/°C-m)	Electric conductivity: σ (S/m)
Specific heat: c_p (J/Kg-°C)	Permitivity: ε (F/m)

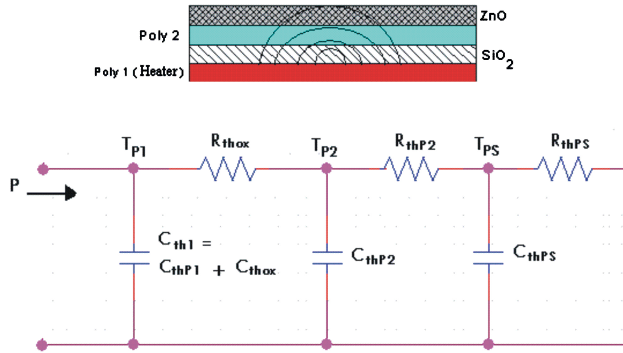

FIGURE 2. Thermo-electric model for the MHP, to study the heat transference within the microhot plate of a MEM gas sensor.

electric to thermal equivalence, and this can be seen in Table I.

Here, a model is developed to anticipate the theoretical thermal response of the MHP as a function of the current applied to the heater. The basis of the model is shown in Fig. 2, where the following considerations were made in order to simplify it: first, the polysilicon heater has a uniform temperature along the suspended diaphragm; second, heat loss across the ends of the heater is not considered since the cross-sectional area of the heater is small compared to its surface area, as well as the heat loss due to the contact between the different layers of the MHP, since they are very thin; and third, the substrate is considered to have a uniform temperature, *Ts*, equal to room temperature, *To*; that is, the substrate is thermally isolated from the MHP, assuming that the cavity avoids temperature diffusion to the Si substrate, as has been practically demonstrated [6]. In Fig. 2, TP1, TP2 and TPS are the nodes representing the temperature in polysilicon 1, polysilicon 2 and the sensor layer (metal oxide thin layer), respectively. Cthp1, Cthox, Cthp2 and Cthps are the thermal capacitances of polysilicon 1, silicon dioxide, polysilicon 2 and the sensor layer, respectively. Finally, Rthox, Rthp2 and Rthps are the thermal resistances of silicon dioxide, polysilicon 2 and the sensor layer, respectively.

The differential equation that describes the transient thermal performance of the microhot plate is, from the heat conduction expression [14],

$$\rho\, c \frac{\partial T}{\partial t} = \nabla \cdot (\kappa\, \nabla T) + J\, \nabla \psi, \tag{1}$$

where κ is the thermal conductivity, ψ is the electric potential, J is the current density, ρ is the material density and c is the specific heat. Equation (1) holds for either conducting or isolating materials of the MHP. The left side of Eq. (1) can be modeled with a capacitance, whose magnitude is the result of integrating the time dependent term [15]

$$\rho\, c \frac{\partial}{\partial t} \int_V T\, dV. \tag{2}$$

The second term on the right represents Joule heating of the polysilicon heater, so that Eq. (1) can be written as follows:

$$C_{th} \frac{\partial T}{\partial t} = \frac{\Delta T}{R_{th}} + I^2 R(T), \tag{3}$$

where C_{th} is the thermal capacitance, R_{th} is the thermal resistance, ΔT represents the temperature difference between the heater and room temperature, I is the electric current through the polysilicon heater and $R(T)$ is its resistance as a function of temperature, since it is well known that the resistance value of this material is temperature dependent [16].

Thermal capacitance and resistance are given by Eqs. (4) and (5):

$$C_{th} = \rho\, c\, V \tag{4}$$

$$R_{th} = \frac{l}{\kappa\, A}, \tag{5}$$

where V is the volume of the material, l is the heat flow direction within the material and A is the cross-sectional area normal to the flow. Having the electric circuit and the expressions of the elements as a function of the material properties, the system can now be thermally analyzed if dimensions are given to the MHP structure. Based on the consideration mentioned above, and making use of Eq. (3), an energy balance of the equivalent circuit can be made to obtain a system of differential equations that can describe the steady state thermal behavior of the sensor structure, as shown next:

$$\begin{aligned} C_{P1} \frac{\partial T_{P1}}{\partial t} &= I^2 R(T) - \frac{T_{P1} - T_{P2}}{R_{OX}} \\ C_{P2} \frac{\partial T_{P2}}{\partial t} &= \frac{T_{P1} - T_{P2}}{R_{OX}} - \frac{T_{P2} - T_{PS}}{R_{P2}} \\ C_{PS} \frac{\partial T_{PS}}{\partial t} &= \frac{T_{P2} - T_{PS}}{R_{P2}} - \frac{T_{PS}}{R_{PS}}. \end{aligned} \tag{6}$$

The sub-index in each term stands for the corresponding node in Fig. 2. The term $R(T)$ in equation (3) can be described by the following expression:

$$R(T) = R_0 \left[1 + \alpha\, (T - T_0)\right], \tag{7}$$

where R_0 is the average resistance at temperature T_0, that will be considered in this case as the room temperature and α is the *Temperature Coefficient of Resistance*, TCR. Then, with the substitution of Eq. (7) into Eqs. (6), we obtain

$$\begin{aligned} \frac{\partial T_{P1}}{\partial t} &= \frac{I^2 R_0}{C_{P1}} + \frac{\alpha\, I^2 R_0}{C_{P1}} T_{P1} - \frac{1}{R_{OX} C_{P1}} T_{P1} \\ &\quad + \frac{1}{R_{OX} C_{P1}} T_{P2} \\ \frac{\partial T_{P2}}{\partial t} &= \frac{1}{R_{OX} C_{P2}} T_{P1} - \frac{1}{R_{OX} C_{P2}} T_{P2} - \frac{1}{R_{P2} C_{P2}} T_{P2} \\ &\quad + \frac{1}{R_{P2} C_{P2}} T_{PS} \\ \frac{\partial T_{PS}}{\partial t} &= \frac{1}{R_{P2} C_{PS}} T_{P2} - \frac{1}{R_{P2} C_{PS}} T_{PS} \frac{1}{R_{PS} C_{PS}} T_{PS}. \end{aligned} \tag{8}$$

To find the solution of the system of equations, the following initial conditions are considered:

$$T_{P1}\,(t=0)=0°C$$
$$T_{P2}\,(t=0)=0°C$$
$$T_{PS}\,(t=0)=0°C. \tag{9}$$

In order to simplify the expressions, the following constants are defined:

$$A{=}\frac{I^2R_0}{C_{P1}}\;;B{=}\frac{\alpha I^2R_0}{C_{P1}}\;;C{=}\frac{1}{R_{OX}C_{P1}}\;;D{=}\frac{1}{R_{P2}C_{P2}};$$
$$E{=}\frac{1}{R_{OX}C_{P2}}\;;F{=}\frac{1}{R_{PS}C_{PS}}\;;G{=}\frac{1}{R_{P2}C_{PS}}. \tag{10}$$

Using Eqs. (10) in equations (8), we obtain

$$\frac{\partial T_{P1}}{\partial t}=A+(B-C)\;T_{P1}+C\,T_{P2}$$
$$\frac{\partial T_{P2}}{\partial t}=E\,T_{P1}-(D+E)\;T_{P2}+D\,T_{PS}$$
$$\frac{\partial T_{PS}}{\partial t}=G\,T_{P2}-(F+G)\;T_{PS}. \tag{11}$$

Again, the next constants can be defined:

$$H=C-B,$$
$$J=D+E,$$
$$K=F+G, \tag{12}$$

from which the system of equations is, finally:

$$\frac{\partial T_{P1}}{\partial t}=A-H\,T_{P1}+C\,T_{P2}$$
$$\frac{\partial T_{P2}}{\partial t}=E\,T_{P1}-J\,T_{P2}+D\,T_{PS}$$
$$\frac{\partial T_{PS}}{\partial t}=G\,T_{P2}-K\,T_{PS}. \tag{13}$$

It is convenient to handle Eqs. (13) as a matrix, as follows:

$$\begin{bmatrix} sT_{P1}(s)\\ sT_{P2}(s)\\ sT_{PS}(s)\end{bmatrix}=\begin{bmatrix}-H & C & 0\\ E & -J & D\\ 0 & G & -K\end{bmatrix}\cdot\begin{bmatrix}T_{P1}(s)\\ T_{P2}(s)\\ T_{PS}(s)\end{bmatrix}+\begin{bmatrix}A(s)\\ 0\\ 0\end{bmatrix}+\begin{bmatrix}T_{P1}(0)\\ T_{P2}(0)\\ T_{PS}(0)\end{bmatrix} \tag{14}$$

or:

$$\begin{bmatrix} s+H & -C & 0\\ -E & s+J & -D\\ 0 & -G & s+K\end{bmatrix}\cdot\begin{bmatrix}T_{P1}(s)\\ T_{P2}(s)\\ T_{PS}(s)\end{bmatrix}=\begin{bmatrix}A(s)\\ 0\\ 0\end{bmatrix}+\begin{bmatrix}T_{P1}(0)\\ T_{P2}(0)\\ T_{PS}(0)\end{bmatrix}, \tag{15}$$

and using the initial conditions (9) in (15),

$$\begin{bmatrix}T_{P1}(s)\\ T_{P2}(s)\\ T_{PS}(s)\end{bmatrix}=\begin{bmatrix} s+H & -C & 0\\ -E & s+J & -D\\ 0 & -G & s+K\end{bmatrix}^{-1}\cdot\begin{bmatrix}A(s)\\ 0\\ 0\end{bmatrix}. \tag{16}$$

Taking the inverse of (16), the matrix is now:

$$\begin{bmatrix} s+H & -C & 0\\ -E & s+J & -D\\ 0 & -G & s+K\end{bmatrix}^{-1}$$
$$=\begin{bmatrix} s^2+s(J+K)+JK-DG & sC+CK & CD\\ sE+EJ & s^2+s(H+K)+HK & sD+DH\\ EG & sG+GH & s^2+s(J+H)+(HJ-EC)\end{bmatrix}\frac{1}{\Delta(s)} \tag{17}$$

where

$$\Delta(s)=\begin{vmatrix} s+H & -C & 0\\ -E & s+J & -D\\ 0 & -G & s+K\end{vmatrix}$$
$$=s^3+s^2(H+J+K)+s(JK+HK+HJ-CE-DG)+(HJK-DGH-CEK) \tag{18}$$

Equation (17) can be also simplified, by defining the following constants:

$$L = H + J + K\,;$$
$$M = JK + HK + HJ - CE - DG\,;$$
$$N = HJK - DGH - CEJ;$$
$$O = J + K\,; \qquad P = CK.$$

Then, Eq. (18) can be expressed as:

$$\Delta(s) = s^3 + Ls^2 + Ms + N. \tag{19}$$

Now, Eq. (16) can be used to solve for $TP1$, which is the temperature present in the polysilicon heater:

$$T_{P1}(s) = \frac{A(s)\cdot\left[s^2 + sO + P\right]}{\Delta(s)},$$

where $A(s) = A/s$, and so

$$T_{P1}(s) = \frac{A\cdot\left[s^2 + sO + P\right]}{(s-0)\,(s-\lambda_1)\,(s-\lambda_2)\,(s-\lambda_3)}, \tag{20}$$

and λ_1, λ_2, λ_3 are the roots of the third degree equation.

Applying partial fraction expansion and the inverse Laplace transform, $TP1$ can be obtained as a function of time:

$$T_{P1}(t) = \Psi_0 + \Psi_1\ell^{\lambda_1 t} + \Psi_2\ell^{\lambda_2 t} + \Psi_3\ell^{\lambda_3 t}, \tag{21}$$

where

$$\Psi_0 = -\frac{A\cdot P}{\lambda_1\cdot\lambda_2\cdot\lambda_3} \quad \Psi_1 = \frac{A\left(r_1^2 + r_1 O + P\right)}{\lambda_1\left(\lambda_1-\lambda_2\right)\left(\lambda_1-\lambda_3\right)}$$
$$\Psi_2 = \frac{A\left(r_2^2 + r_2 O + P\right)}{\lambda_2\left(\lambda_2-\lambda_1\right)\left(\lambda_2-\lambda_3\right)}$$
$$\Psi_3 = \frac{A\left(r_3^2 + r_3 O + P\right)}{\lambda_3\left(\lambda_3-\lambda_1\right)\left(\lambda_3-\lambda_2\right)}$$
$$\lambda_1 = \frac{Y_1 - L}{3} \quad \lambda_2 = \frac{Y_2 - L}{3} \quad \lambda_3 = \frac{Y_3 - L}{3}$$
$$Y_1 = \sqrt[3]{U} + \sqrt[3]{V} \quad Y_2 = w\,\sqrt[3]{U} + w^2\,\sqrt[3]{V}$$
$$Y_3 = w^2\,\sqrt[3]{U} + w\,\sqrt[3]{V}$$
$$w = \frac{-1+\sqrt{-3}}{2} \quad U = -\frac{R}{2} + \sqrt{\frac{R^2}{4} + \frac{Q^3}{27}}$$
$$V = -\frac{R}{2} - \sqrt{\frac{R^2}{4} + \frac{Q^3}{27}}$$
$$Q = 9M - 3L^2 \quad R = 27N - 9LM + 2L^3.$$

Finally, the solution of equations (8) with initial conditions (9) is given by the following expressions:

$$T_{P1}(t) = \Psi_0 + \Psi_1\ell^{\lambda_1 t} + \Psi_2\ell^{\lambda_2 t} + \Psi_3\ell^{\lambda_3 t}$$

$$T_{P2}(t) = \frac{1}{C}\left[\lambda_1\Psi_1\ell^{\lambda_1 t} + \lambda_2\Psi_2\ell^{\lambda_2 t} + \lambda_3\Psi_3\ell^{\lambda_3 t} - (B-C)\,T_{P1}(t) - A\right]$$

$$T_{PS}(t) = \frac{1}{D}\left[\frac{dT_{P2}(t)}{dt} + (D+E)T_{P2}(t) - ET_{P1}(t)\right]. \tag{22}$$

These expressions define temperatures $TP1$, $TP2$ and TPS in the respective nodes of the electric circuit shown in Fig. 2, at any time. From Eq. (22), temperature $TP1$ at an infinite time is

$$T_{P1}(\infty) = \Psi_0; \tau_1 = \frac{1}{|\lambda_1|}; \quad \tau_2 = \frac{1}{|\lambda_2|}; \quad \tau_3 = \frac{1}{|\lambda_3|}$$

If a rectangular current pulse is applied to the polysilicon heater, the time dependence of temperature can be described as follows:

$$T_{P1}(t) = T_{P1}(\infty) - |\Psi_1|\,\ell^{-\frac{t}{\tau_1}} - |\Psi_2|\,\ell^{-\frac{t}{\tau_2}} - |\Psi_3|\,\ell^{-\frac{t}{\tau_3}}. \tag{23}$$

Then, to finally plot the variation of temperature when the heater is excited with a rectangular current pulse, thermal resistances and capacitances must be calculated regarding the material used in the structure. This can be done with the following expressions:

$$R_{th} = \frac{L}{\kappa A}, \tag{24}$$

$$C_{th} = m\cdot c_e, \tag{25}$$

$$m = \rho\cdot V, \tag{26}$$

where L is the length, in m; κ is the thermal conductivity, in W/°C-m; A is the cross-sectional area, in m^2; m is the mass of the material, in Kg; ρ is its density, in Kg/m^3; V is the volume, in m^3 and c_e is the specific heat in W-sec/Kg-°C. Table II shows the values of these parameters for the materials used in the technology considered [17,18].

Using Eqs. (24)-(26) with the parameters listed in Table II will result in the following values of thermal resistances and capacitances for each layer:

$$C_{P1} = 3.5014\,n\,Wseg/^\circ C \tag{27}$$

$$C_{ox} = 1.6991\,n\,Wseg/^\circ C \tag{28}$$

$$C_{th1} = C_{P1} + C_{ox} \tag{29}$$

$$C_{th1} = 5.2005\,n\,Wseg/^\circ C \tag{30}$$

$$R_{OX} = 4.3208\,^\circ C/W \tag{31}$$

$$C_{P2} = 15.73n\,Wseg/^\circ C \tag{32}$$

$$R_{P2} = 2.9412\,^\circ C/W \tag{33}$$

$$C_{PS} = 4.7529\,n\,Wseg/^\circ C \tag{34}$$

$$R_{PS} = 4.1152\,^\circ C/W. \tag{35}$$

TABLE II. Parameters of the different layers of the MHP structure.

Parameter	Value	Parameter	Value	Parameter	Value
ρ_p	2320 Kg/m^3	t_{p2}	1 μm	c_{ps}	523.35 J/Kg±C
c_p	678 J/Kg °C	ρ_{ox}	2200 Kg/m^3	κ_{ps}	6 W/m ±C
κ_p	34 W/m-°C	c_{ox}	730 J/Kg-°C	w_{ps}	90 ^{1}m
w_{p1}	10 μm	κ_{ox}	1.4 W/m-°C	l_{ps}	90 ^{1}m
l_{p1}	371 μm	w_{ox}	115 μm	t_{ps}	200 nm
t_{p1}	600 nm	l_{ox}	115 μm	α	1.0835 × 10^{-3} ±C^{-1}
w_{p2}	100 μm	t_{ox}	80 nm	R_0	1545
l_{p2}	100 μm	ρ_{ps}	5606 Kg/m^3	T_0	27 ±C

$t_{p1,p2,ox}$: layer thickness; $l_{p1,p2,ox}$: layer length; $w_{p1,p2,ox}$: layer width.

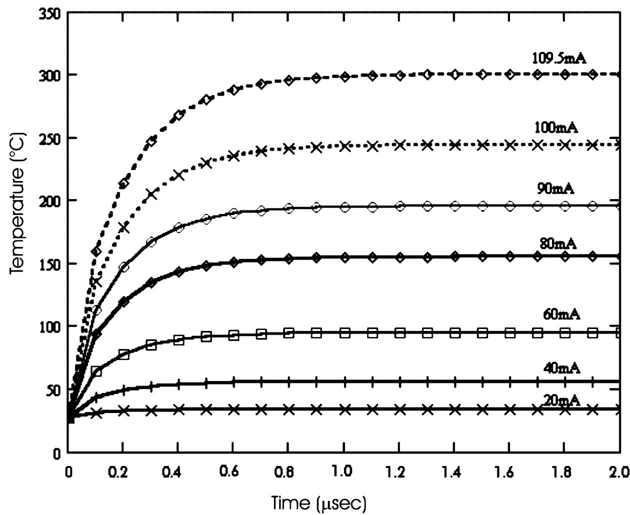

FIGURE 3. Temperature response of the heater as a function of time.

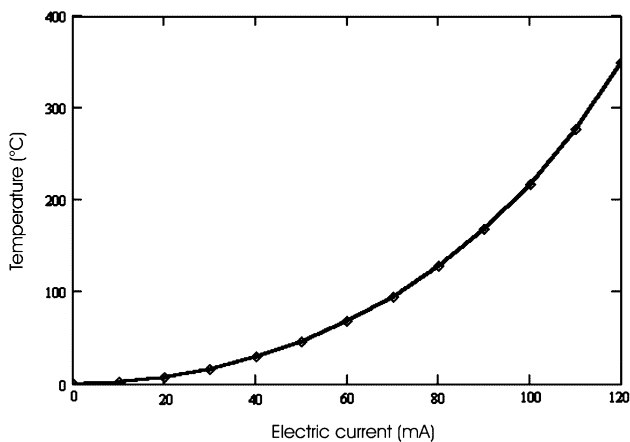

FIGURE 4. Temperature response as a function of applied current.

Figure 3 shows the plot of Eq. (23) at different levels of rectangular current pulses, from which it can be seen that 109.5 mA should be applied in order to reach 300°C in the polysilicon heater, for the dimensions selected in this design. The time it takes for the temperature to rise from room temperature to the temperature set by the applied current is about 1.2 μsec. When designing the electronic circuits, this analysis is useful for choosing the appropriate electronic configuration for the current source that will be used to power the heater. This current source should be integrated together with the controlling circuit for the heater in the sensor system, placed in the same chip. In this analysis, 300°C is used as the target temperature, since it was established as the best temperature for the reaction between the gas and the sensor layer, to take place [18]. On the other hand, Fig. 4 shows now the plot of Eq. (23) as a function of the current applied.

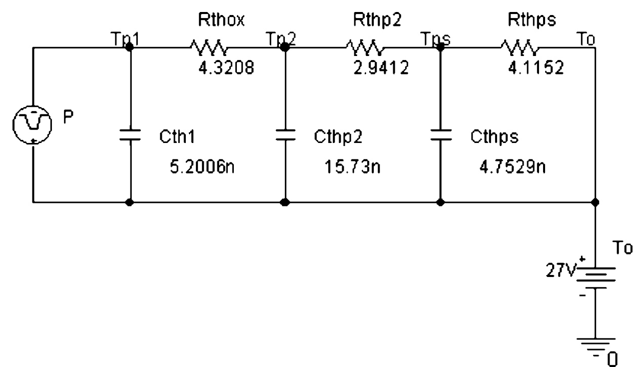

FIGURE 5. Equivalent electric circuit for the MEM gas sensor.

2.2. Simulation with SPICE

The model shown in Fig. 2 can be simulated with SPICE, which is a commonly used software, for circuit analysis. The values used for the thermal resistances and capacitances present in the circuit are also those calculated in the above section and configuring the current source with square pulses. As shown in Table I, the parameter of voltage is equivalent to temperature, so we are interested in the potential at node TPS; but the circuit should include an extra DC source that will be the reference, instead of ground, and will be considered as room temperature and is represented in Fig. 5. For the

simulation of the circuit, a 50% duty cycle of 1 KHz was arbitrarily used, but this can be varied if an exhaustive analysis is desired to see the effect of using different types of pulses or waveforms. Therefore, the results presented here are for these particular considerations, but can be different depending on what the designer has in mind for the system.

Figure 6 shows the result of the simulation, where a magnitude of 24 A is enough to reach the target temperature of 300°C. It should be remembered here that the *y-axis*, given in volts, is likely to temperature, but also, that the current source used to drive the circuit, stands for the heat flow in the thermal equivalence. This is the same as the power dissipated by the polysilicon heater and is calculated using the following equation:

$$P\left(T\right)=I^{2}R\left(T\right) \tag{36}$$

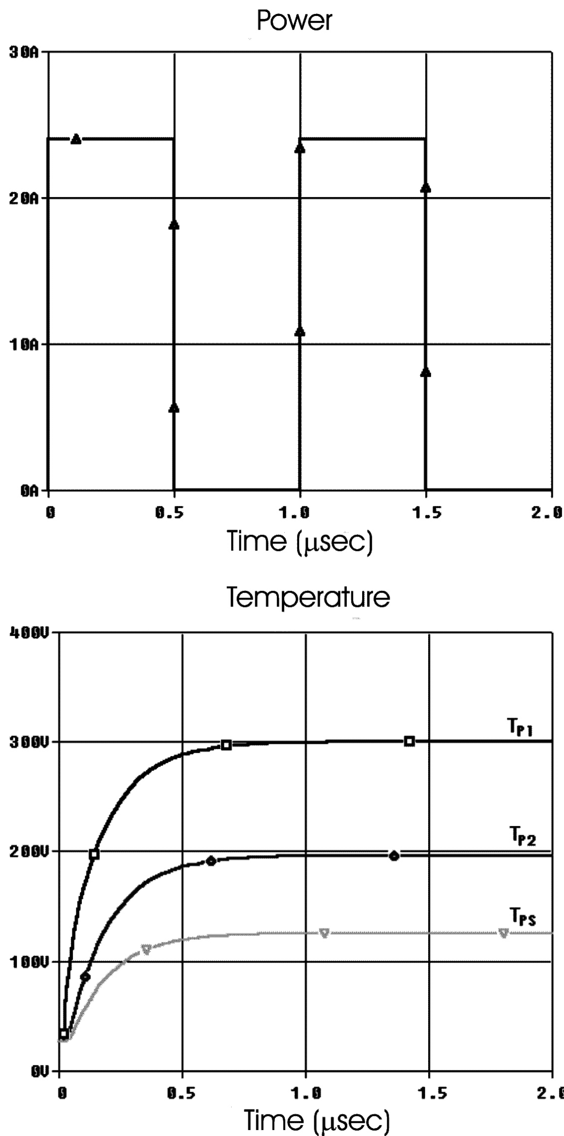

FIGURE 6. Temperature increase in nodes TP1, TP2 and TPS with a rectangular current pulse of 24 A, 50 % duty cycle and 1 KHz of frequency.

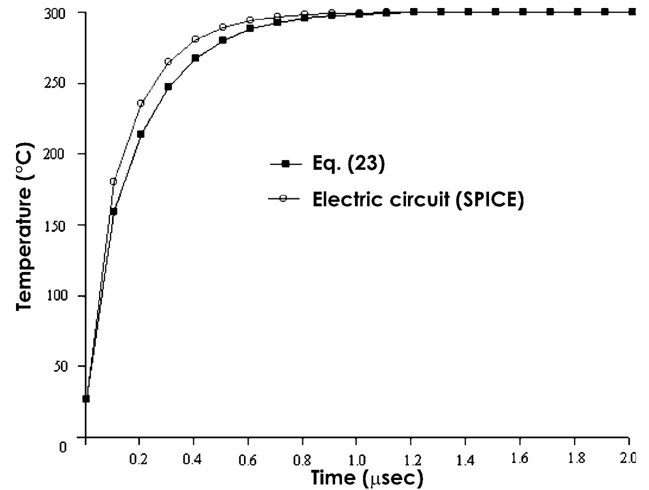

FIGURE 7. Comparison of the temperature response of the heater with Eq. (23) and the equivalent electric circuit of Fig. 2.

Using Eq. (7) and the values of α and R_0 shown in Table II, the result for a 300°C temperature is

$$R\left(300^{\circ}C\right)=2.002k\Omega$$

Solving Eq. (36) for I, the current derived from the simulation is 109.49 mA, the same as that which was found analytically. Again, this can be different if other waveform for exciting the circuit is chosen and should give another current magnitude. Finally, comparing the analytical solution with that given by the simulation gives the same result, as can be seen in Fig. 7. For this design, the response time for increasing the heater from room temperature to 300°C is about 1.2 μsec. Thus, it can be concluded that the analytical model is appropriate for the microhot plate design, together with the circuit used.

2.3. Heat transference model

Another important concern in the performance of the microhot plate is its thermal efficiency. Power consumption should be minimized if the objective is to integrate the sensor with the signal conditioning and control electronics. As high currents are needed to reach high temperatures in the sensor layer, as shown in the above section, it is important to establish the parameters of the microhot plate that influence directly in power dissipation. This is closely related to heat transfer in the system since heat is dissipated across the system, the same time as it is generated. Then, regarding to the electric power applied to the heater, it is dissipated by three mechanisms: a) heat conduction to the structure surrounding the MHP; b) heat conduction to the air; and c) radiation. Heat conduction to the air is lost by convection due to the interaction between a solid and a fluid. When the MHP reaches a steady state temperature, electric power consumption must be equal to the heat loss, P_{mc}, and can be expressed in terms of the previous mechanisms:

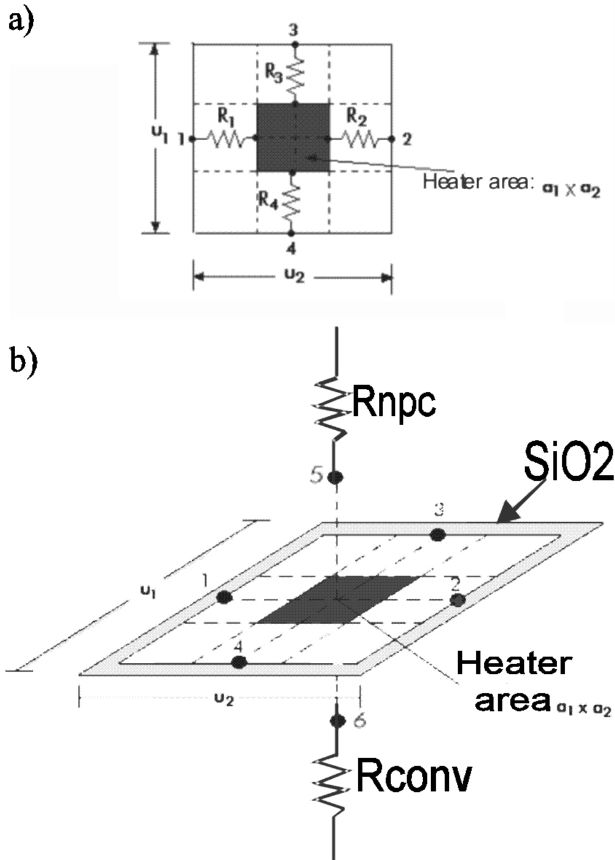

FIGURE 8. MHP model to consider heat loss by: a) conduction and b) convection.

$$P_{mc}=a_{cond}(T-T_0)+b_{conv}(T-T_0)^2+c_{rad}\left(T^4-T_0^4\right), \quad (37)$$

where a, b and c are constants related to heat loss by conduction, convection and radiation, respectively. The last type of heat loss is negligible in devices operated at high temperatures and will not be considered [19]. To analyze the thermal behavior in a steady state of the MHP, a system similar to that shown in Fig. 8 will be used to derive an equivalent circuit that models heat loss by conduction and convection.

As established in Eq. (5), the resistance elements in Fig. 8a can be expressed in terms of thermal conductivity, considering heat loss by conduction:

$$R_1 = R_2 = R_3 = R_4 \frac{\delta}{k_{ox} * A_{cond}}, \quad (38)$$

where δ is the distance of heat flow between the heater and the suspended diaphragm of SiO_2, κ_{ox} is the thermal conductivity of silicon dioxide, and A_{cond} is the cross-sectional area between both materials. Considering the dimensions shown in Fig. 8, Eq. (38) is then written as:

$$R_1 = \frac{\frac{u_2}{2} - \frac{a_2}{2}}{k_{ox} * t_{ox} * a_1} = \frac{u_2 - a_2}{2 * \kappa_{ox} * t_{ox} * a_1} \quad (39)$$

Specifically, u_2 is the silicon dioxide layer length, t_{ox} is its thickness, a_1 and a_2 are the heater length and width, respectively. From the nodal system in Fig. 8, and taking into consideration Eq. (38), it follows that:

$$R_{cond} = R_1 // R_2 // R_3 // R_4 \quad (40)$$

$$R_{cond} = \frac{u_2 - a_2}{8 \cdot k_{ox} \cdot t_{ox} \cdot a_1} \quad (41)$$

From Fig. 8 also, R_{conv} and R_{mpc} are the resistive elements that represent the heat loss by convection to the cavity and to the air, respectively. This kind of resistance is expressed in terms of the heat transference coefficient of the material, h, given in *W/°C-m*^{2} and A_{SiO2} is the exposed area from which the heat flows, given in m^2. The former is expressed as follows:

$$R_{conv} = \frac{1}{h \cdot A_{SiO2}} \quad (42)$$

and the latter, is the sum of the series combination of the individual thermal resistances due to conduction, of silicon dioxide, R_{ox}, polysilicon II, R_{P2}, sensor layer R_{SL} and the resistance due to convection to the air, R_{conv1}. Since in this kind of structure the layers are normally thin, conduction is considered negligible compared to convection, so that:

$$R_{mpc} = R_{ox} + R_{P2} + R_{SL} + R_{conv1} \quad (43)$$

$$R_{conv1} \gg R_{ox} + R_{P2} + R_{SL}$$

$$R_{mpc} = R_{conv1}$$

$$R_{mpc} = \frac{1}{h \cdot A_{SL}}, \quad (44)$$

where A_{SL} is the area of the metal oxide layer, in m^2.

On the other hand, the elements in the system store heat as well, and this can be considered with the thermal capacitance, C_{th}, to take advantage of the electric equivalence of the thermal system. In this case, this capacitance is represented between the node at which the heat is generated and the node at which heat is dissipated, that is, the air outside the sensor. Then, the simplified circuit shown in Fig. 9 will represent the system from which a transient and steady state analysis can be made. T_{mc} and T_0, are the temperature in the heater and room temperature, respectively; C is the thermal capacitance of the MHP, R_{cond}, is the resistance due to heat flow from the heater to the silicon dioxide beneath it, R_{mpc} is the thermal resistance (convection) of the MHP, and R_{conv} is the thermal resistance due to convection to the etched cavity in the substrate.

From Fig. 9, heat flow will result in the following expression:

$$C\frac{dT_{mc}}{dt} = P_{mc} - \Delta T\left(\frac{1}{R_{cond}} + \frac{1}{R_{mpc}} + \frac{1}{R_{conv}}\right), \quad (45)$$

where $\Delta T = (T_{mc} - T_0)$.

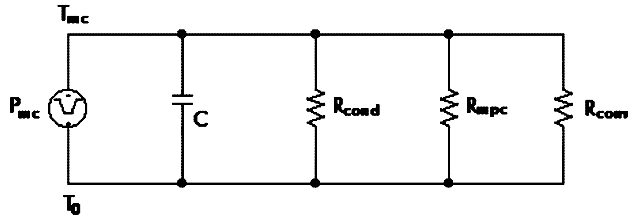

FIGURE 9. Equivalent electric circuit for transient and steady state analysis.

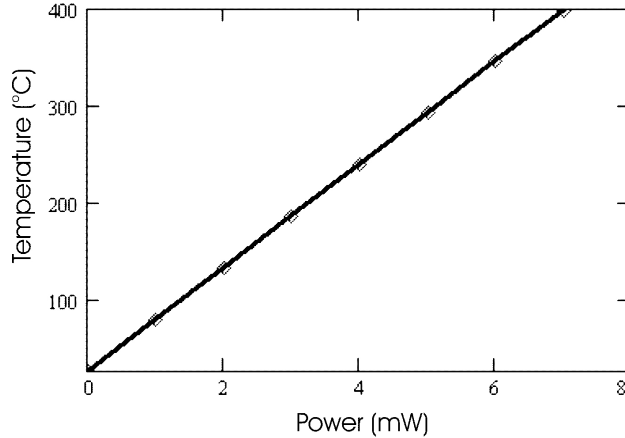

FIGURE 10. Temperature as a function of applied power to the MHP.

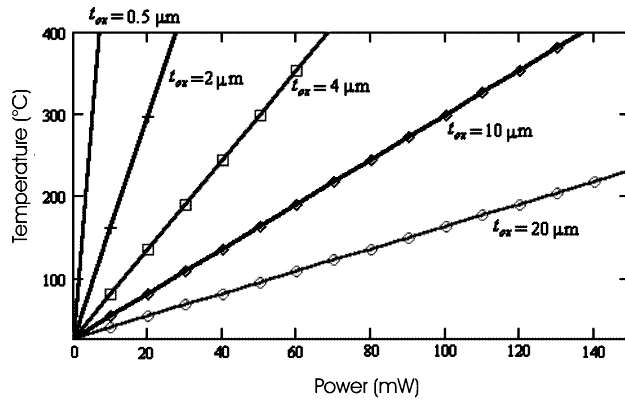

FIGURE 11. Temperature as a function of applied power to the MHP, with different oxide thickness.

Using (41), (42) and (44) in (45),

$$C\frac{dT}{dt} = P_{mc} - \Delta T\left(\frac{8\cdot k_{ox}\cdot t_{ox}\cdot a_1}{u_2 - a_2} + h\cdot A_{PS} + h\cdot A_{S_iO_2}\right). \quad (46)$$

To consider the steady state condition of the system, the term on the left side of Eq. (46) must be made equal to zero, and finally, the power dissipation of the system as a function of ΔT can be obtained:

$$P_{mc}{=}\Delta T\left(\frac{8\cdot k_{ox}\cdot t_{ox}\cdot a_1}{u_2{-}a_2}{+}h\cdot A_{PS}{+}h\cdot A_{S_iO_2}\right). \quad (47)$$

Using the coefficients of the materials involved and their geometries as shown in Table II, with h=15 W/m^2-°C, Eq.(47) can be plotted as shown in Fig. 10.

The inverse of the slope of the line in Fig. 10 gives the thermal efficiency, η:

$$\eta = \frac{\Delta T}{\Delta P}, \quad (48)$$

and from the plot, the thermal efficiency for the design presented is

$$\eta = \frac{360°C - 150°C}{6mW - 2mW} = 52.5°C/mW. \quad (49)$$

The results from Eq. (47) may be different if different thicknesses of the layers are considered. For instance, for different values of thickness in the SiO_2 layer between the polysilicon layers (since it has the highest thermal resistance), the thermal efficiency can be increased or decreased, as shown in Fig. 11.

From Fig. 11, it can be seen that thermal efficiency is inversely proportional to the layer thickness, so that the technological issues are closely related to this parameter and, if possible, it must be considered when designing a MHP if the goal is to minimize the power consumption.

Finally, using the circuit of Fig. 9 again, the thermal constant for the system being considered can be found from the following equation:

$$\tau = \frac{C}{G_{cond} + G_{conv} + G_{mpc}}, \quad (50)$$

where

$$C = C_{P1} + C_{OX} + C_{P2} + C_{PS}, \quad (51)$$

which can be calculated with the coefficients of Table II and G=1/R. Then, the value for the thermal constant is τ=1.36 msec. Again, this depends on the geometry and dimensions of the layers used in the system and can be adjusted to optimize it.

3. Conclusions

A model for the consideration of the geometry and type of structure that can be used with a microhot plate applied to gas sensors was developed. This model can be useful in calculating or simulating the temperature performance when a current source is powering the heater of polysilicon and therefore, it is possible to optimize the structure depending on the technology from which the microhot plate will be fabricated, for example, the thickness of the different layers and the materials used, including the sensor layer. The fact it placing the microhot plate over a suspended diaphragm by MEMS technology also helps to integrate the sensor structure with the signal and controlling electronics, even when the sensor works at 300°C, since this temperature will be isolated from the rest of the electronics, within the substrate, due to the

poor heat transfer characteristics of the cavity. The power consumption of the entire system can be optimized as well, since one main objective for the performance of the sensor is to obtain a high thermal efficiency by minimizing the power used by the bias source.

1. S.J. Pearton, D.P. Norton, K. Ip and Y.W. Heo, *J.Vac. Sci. Technol. B* **22** (2004) 932.
2. J. Brezmes *et al.*, *IEEE Sensors Journal* **5** (2005) 97.
3. J. S. Suehle, M. Gaitan, and S. Semancik, *IEEE Electron Device Letters* **14** (1993) 118.
4. D. Vincenzi *et al.*, *J. Vac. Sci. Technol. B* **18** (2000) 2441.
5. M.Y. Agridi *et al.*, *IEEE Sensors Journal* **2** (2002) 644.
6. M. Graf *et at.*, *IEEE Sensors Journal* **4** (2004) 9.
7. D. Barrentino *et at.*, *Proceedings IEEE Int. Symp. on Circ. and Syst., ISCAS* **2:157** (2002) II-157.
8. J. Laconte, C. Dupont, D. Flandre, and J.-P. Raskin, *IEEE Sensors Journal* **4** (2004) 670.
9. D. Barrentino *et at.*, *IEEE Journal of Solid-State Circuits* **39** (2004) 1202.
10. J.C. Belmonte *et al.*, *Sensors and Actuators B* **114** (2006) 881.
11. O. Brand and G.K. Fedder, *Advanced Micro & Nanosystems* Ed. Wiley-VCH (2005).
12. Y. Amemiya, T. Ono, and K. Kato, *IEEE Trans. Electron Devices* **ED-26** (1979) 1738.
13. C.H. Mastrengelo, J.H. Yeh, and R.S. Muller, *IEEE Trans. Electron Devices* **39** (1992) 1363.
14. Tai-Ran Hsu, *MEMS & Microsystems. Design and Manufacture* McGraw Hill (2002).
15. M. Necati Osizik, *Boundary Value Problems of Heat Conduction* Dover Publications, Inc, Minoela, (New York 1968) 262.
16. P.E. Allen and D.R. Douglas, *CMOS Analog Circuit Design* Saunders College Publishing (1987).
17. W. Gardner Julian, *Microsensors, MEMS and Smart Devices* John Wiley and Sons (2001).
18. J.L. Gonzalez Vidal, A. Reyes Barranca, M de la L. Olvera, A. Maldonado, and W. Calleja Arriaga, *Smart Sensors and Actuators, and MEMS II, Proc. Of SPIE* **5836** (2005) 247.
19. Jr-Hung Tsai and Liwei Lin, *Journal of Heat Transfer* **124** (2002) 375.